Eur Radiol (2003) 13:1820–1835
DOI 10.1007/s00330-003-1902-z

Klaus Woertler

Benign bone tumors and tumor-like lesions: value of cross-sectional imaging

Received: 24 January 2003
Accepted: 21 March 2003
Published online: 17 April 2003

K. Woertler (✉)
Department of Radiology,
Technische Universität München,
Klinikum rechts der Isar,
Ismaninger Strasse 22, 81675 Munich,
Germany
e-mail: woertler@roe.med.tu-muenchen.de
Tel.: +49-89-41402696
Fax: +49-89-41404834

Abstract This article reviews the role of CT and MR imaging in the diagnosis of benign bone tumors and tumor-like lesions of bone with with regard to differential diagnosis, the assessment of tumor-related complications, and the detection of postoperative recurrence. Indications for cross-sectional imaging of specific lesions, including osteoid osteoma, osteoblastoma, enchondroma, osteochondroma, intraosseous lipoma, hemangioma, giant cell tumor, aneurysmal bone cyst, simple bone cyst, and eosinophilic granuloma, are discussed, and advantages and disadvantages of the different imaging modalities are illustrated on the basis of pathologically confirmed cases.

Keywords Bone neoplasms · Diagnosis · Computed tomography · Magnetic resonance imaging

Introduction

The inhomogeneous group of benign bone lesions (Table 1) includes true neoplasms (bone tumors) as well as several tumor-like lesions of bone, which represent non-neoplastic conditions that can simulate the appearance of benign or malignant bone tumors [1, 2, 3, 4].

The majority of benign true neoplasms of bone are detected in children and young adults. Benign bone tumors can be classified according to their matrix production and/or predominant cell type into bone-forming, cartilage-forming, connective-tissue, and vascular lesions. Semimalignant lesions, such as giant cell tumor and ameloblastoma, are also summarized under this entity. With the exception of osteoid osteomas, osteochondromas, and enchondromas, which together account for approximately 20% of all primary bone tumors, and the relatively frequent hemangiomas of the spine, most of these lesions are very rare [1, 3, 4].

The term "tumor-like lesions of bone" summarizes various conditions of non-neoplastic nature originating from or affecting the bone and presenting as solitary or sometimes multiple bone lesions. The most important lesions of this group are listed in Table 1; however, many more, even congenital, inflammatory, ischemic, and traumatic disorders, can appear in this fashion and therefore could be added to this selection. Different fibro-osseous and cystic lesions represent the most common entities in this group with nonossifying fibroma, simple and aneurysmal bone cyst being the most frequent [2, 3, 4].

Although the diagnosis of bone tumors often represents a "team diagnosis" elaborated by and necessitating close cooperation of orthopedic surgeons, radiologists, and pathologists, the radiologist's contribution is the most responsible and most important in cases of benign bone lesions. The primary aim of imaging should be a specific diagnosis (in the ideal case obviating the need for biopsy) or narrowing of the differential diagnosis, in order to decide whether biopsy, surgical intervention, or simple observation are required for further management.

Many articles and book chapters have emphasized the importance of plain radiography as the single most valuable imaging modality in the diagnosis of bone lesions. This article reviews the value of cross-sectional imaging techniques in patients with benign bone tumors and tumor-like lesions for differential diagnosis, the assessment of tumor-related complications, and the detection of postoperative recurrence.

Table 1 Benign bone tumors and tumor-like lesions (selection)

Benign bone tumors	Tumor-like lesions
Bone-forming tumors	Fibro-osseous lesions
Osteoma	Non-ossifying fibroma
Osteoid–osteoma	Fibrous dysplasia
Osteoblastoma	Osteofibrous dysplasia
	Periosteal desmoid
Cartilage-forming tumors	
Enchondroma	Cystic lesions
Osteochondroma	Simple bone cyst
Periosteal chondroma	Aneurysmal bone cyst
Chondroblastoma	Intraosseous ganglion
Chondromyxoid fibroma	Epidermoid cyst
	Subchondral cyst
Connective-tissue tumors	
Desmoplastic fibroma	Giant-cell-containing lesions
Benign fibrous histiocytoma	Giant cell reparative granuloma
Ossifying fibroma	Brown tumor
Myxoma	Pigmented villonodular synovitis
Lipoma	
	Others
Vascular tumors	Eosinophilic granuloma
Hemangioma	Pseudotumors
Lymphangioma	
Glomus tumor	
Others/semimalignant	
Giant cell tumor	
Ameloblastoma	

Differential diagnosis

General principles

Since many bone tumors and tumor-like lesions of bone show a predilection for special age groups or anatomic sites, the first step in the diagnosis of such lesions is considering these data [1, 2, 3]. Clinical information concerning the patient's history, presence and duration of symptoms, physical examination, and laboratory findings should also be evaluated [1, 2, 3]. Conventional radiography remains the first imaging modality in evaluation of the localization of a lesion with respect to the longitudinal and axial planes of the involved bone and in determination of its biologic activity by analyzing the patterns of bone destruction and periosteal response [3]. Skeletal scintigraphy, in our experience, is less important in assessment of solitary lesions, but can add valuable information in case of polyostotic involvement (e.g., fibrous dysplasia).

Many benign bone tumors and tumor-like lesions of bone can sufficiently be diagnosed by means of radiography and do not require additional imaging or biopsy. If the combination of clinical and radiographic findings does not allow a specific diagnosis, biopsy is usually mandatory, and both, radiographic and histologic findings together, have to be combined to make the final diagnosis [1, 3].

Computed tomography

In the diagnosis of solitary bone lesions CT is typically used in order to obtain "radiographic" information, where conventional radiographs fail due to limited contrast resolution, complex skeletal anatomy (e.g., spine, pelvis), or superposition of skeletal elements (e.g., scapula). Computed tomography has widely replaced conventional tomography, and recently, with the advent of multislice techniques, it has developed into a "true" multiplanar modality. Computed tomography is superior to radiography in determination of the epicenter of a bone lesion (medullary, cortical, periosteal, parosteal) [3, 4, 5]. The site of origin can be characteristic for a special entity (e.g., non-ossifying fibroma, periosteal chondroma), and it can influence the growth pattern of the lesion, and therefore, it can determine whether the lesion appears more or less aggressive [3]. The biologic activity of a lytic bone lesion is mirrored in its pattern of bone destruction. Independent of the anatomic site of the lesion, CT can define the margins of an osseous defect in 360° survey, it can exactly determine the width of the zone of transition between normal and abnormal bone, and it can detect delicate sclerotic reactions [3, 5]. The most important advantage of CT over radiography probably is its superior delineation of cortical alterations [3, 5], of which cortical expansion and remodeling, endosteal scalloping, and focal penetration represent the most common forms in benign bone lesions. Periosteal reactions represent another barometer of the biologic activity of bone tumors and tumor-like lesions. Computed tomography has the ability to depict periosteal reactions that might be invisible on radiographs due to superposition or limited contrast resolution [3, 5]. Furthermore, CT represents the most valuable imaging modality in detection of subtle matrix calcifications and therefore can be useful in confirming the diagnosis of a bone- or cartilage-forming tumor [1, 3, 4, 5, 6].

MR imaging

Magnetic resonance imaging is generally accepted as the most valuable method in definition of the extent of bone tumors, but it is thought to be less specific in differential diagnosis [7]. In our experience, MR imaging in addition to radiography can at times be very helpful in differential diagnosis of benign bone lesions.

Bone as a tissue shows a relatively uniform response to a growing lesion, which is determined by its growth rate, but one has to keep in mind that the biologic activity of a bone lesion does not necessarily mirror its dignity [3]. Radiographic methods reveal the response of the involved bone but provide limited information on the nature of the underlying process. Although MR imaging has less potential to show different patterns of bone de-

Fig. 1a–f Intraarticular osteoid osteoma of the humerus in a 23-year-old man. **a** Lateral radiograph shows a solid periosteal reaction (*arrow*) at the anterior cortex above the coronoid fossa. **b** Sagittal T1-weighted spin-echo (SE), **c** sagittal short tau inversion recovery (STIR), and **d** axial T2-weighted fast spin-echo (FSE) MR images show an intracortical nidus (*arrowheads*) of predominantly low signal intensity. Note extensive bone marrow and soft tissue edema as well as swelling of the joint capsule and joint effusion on STIR image. **e** Axial CT scan and **f** sagittal reconstruction image clearly show a heavily mineralized nidus (*arrowhead*) within the anterior cortex accompanied by sclerosis of adjacent cancellous bone and a solid periosteal reaction (*arrow*)

Table 2 Tissue characterization in solitary bone lesions

	Radiography	CT	MRI
Osteogenic	++[a]	++[a]	+
Chondrogenic	++[a]	++[a]	+++
Fatty	–	+++	+++
Vascular	–	–	++
Cystic	–	+	+++
Fibrous	–	–	+
Hemosiderotic	–	–	+++

[a] If mineralized

struction and response, due to its superior soft tissue contrast it has the ability to reveal the pathologic anatomy of the underlying process [3, 7].

In addition to morphologic information, MR imaging can be used for tissue characterization by evaluation of signal intensities with different pulse sequences (e.g., lipomatous lesions) and patterns of contrast enhancement (e.g., cartilaginous tumors).

Compared with radiography and CT, MR imaging has proved to be especially advantageous in identification of non-mineralized chondroid matrix, vascular tissue, cysts, and hemosiderotic tissue (Table 2).

Cross-sectional imaging of specific lesions

As mentioned previously, many benign bone tumors and tumor-like lesions, e.g., most connective-tissue tumors and fibro-osseous lesions of bone, can reliably be diagnosed by radiography, and do not require further imaging. In the following, we discuss and illustrate a selection of lesions in which we consider cross-sectional imaging as an additional modality helpful or even necessary.

Osteoid osteoma

Osteoid osteomas most often are located in or close to the cortex of long tubular bones and present with pain at rest that becomes more severe at night and often responds to analgetics [1, 4, 6, 8, 9, 10]; however, the nidus, which represents a hypervascular, bone-forming lesion of 1.5 cm in maximum diameter, is often invisible on radiographs [4]. Furthermore, lesions located in the axial skeleton or small bones and those with a medullary, subperiosteal, or intraarticular localization in long bones can demonstrate uncharacteristic or misleading radiographic features, and therefore, additional cross-sectional imaging is usually required to establish the diagnosis (Fig. 1) [6, 8, 9, 10].

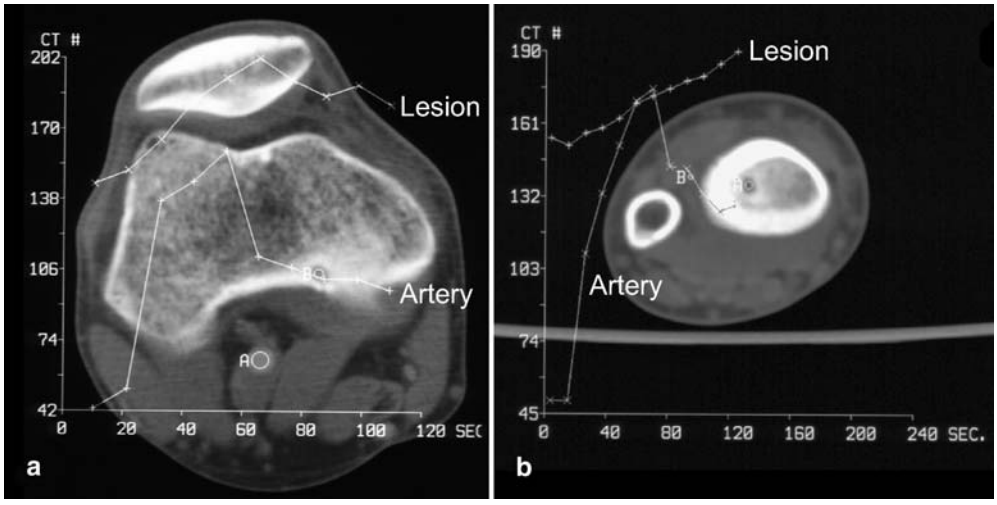

Fig. 2a, b Dynamic CT. **a** Intramedullary osteoid osteoma of the distal femur: the nidus shows arterial peak enhancement followed by washout, which parallels enhancement within the popliteal artery. (From [10]). **b** Brodie's abscess of the distal radius: the lesion demonstrates gradual enhancement and absence of arterial peak. Note morphologic similarity between the two lesions

Computed tomography has proved to be the most valuable method in detection of the nidus, which presents as a well-defined lesion within an area of reactive sclerosis [6, 9, 11, 12]. In more than half of the cases the nidus contains some mineralization, it appears purely osteolytic in approximately one-third of cases, and sometimes it can be completely calcified [6]. If the nidus is located in cancellous bone, CT morphology alone may not allow differentiation of osteoid osteoma from chronic osteomyelitis (Brodie's abscess); however, since the nidus in osteoid osteoma shows marked vascularity and the nidus in chronic osteomyelitis represents an intraosseous abscess, the two entities demonstrate different enhancement patterns on dynamic CT. Osteoid osteoma usually shows early peak enhancement that parallels enhancement of neighboring arterial vessels, whereas Brodie's abscess demonstrates slow and gradual enhancement or even no measurable contrast uptake at all (Fig. 2) [13, 14]. Especially prior to CT-guided percutaneous treatment by means of thermocoagulation or drilling, where histologic verification can be difficult to obtain, dynamic CT has proved to be valuable in distinction of the two conditions [10].

On MR imaging, the nidus tissue can show various signal intensities from isointense to muscle on T1- and hyperintense on T2-weighted images to hypointense on images of all pulse sequences, depending on the amount of matrix production and mineralization [6, 8, 9]. Hypervascularization of the nidus can be demonstrated by gadolinium-enhanced images. Bone marrow and periosteal edema are typically seen in the surrounding of the lesion [9, 11] and are often very pronounced with fat-suppressed T2-weighted, short tau inversion recovery (STIR), and contrast-enhanced T1-weighted pulse sequences (Fig. 1). MR imaging in osteoid osteoma is generally thought to be less specific than CT [9, 11]. Diagnostic errors can occur due to misinterpretation of reactive changes as signs of malignancy, inflammation, or previous trauma. The nidus can easily be overlooked, especially if it is heavily mineralized, and therefore presents with similar low signal intensity as cortical bone or reactive sclerosis. Furthermore, intraarticular osteoid osteomas may not be recognized on MR images, because prominent synovitis and joint effusion are misinterpreted as signs of arthritis and not as reactive phenomena of an intracapsular nidus; however, in our opinion the main sources of error are a non-optimized MR technique [11] and the interpretation of MR images without corresponding radiographs.

Osteoblastoma

Osteoblastoma differs from osteoid osteoma in having a nidus larger than 1.5 cm in diameter and usually showing more variable histologic features [1, 4]. Since approximately one-third of the lesions are located in the spine, where they most often originate from the posterior vertebral elements, and radiographic features of tumors located in long and small bones can be unspecific, cross-sectional imaging is mandatory in characterization of the lesion and local staging in the majority of cases [1, 4, 6, 15, 16].

Computed tomography can aid in differential diagnosis by depiction of osteogenic matrix mineralizations or a thin shell-like periosteal reaction surrounding an expansile osteolytic lesion, which is most often observed in spinal osteoblastomas (Fig. 3) [6, 12, 15, 16].

On MR images osteoblastomas often show unspecific findings with various signal intensities [15]. Hypointensity with all pulse sequences has been reported to occur in lesions with mineralization of the matrix as well as in non-mineralized tumors which on histologic examination showed diffuse osteoid production [16]. Corresponding

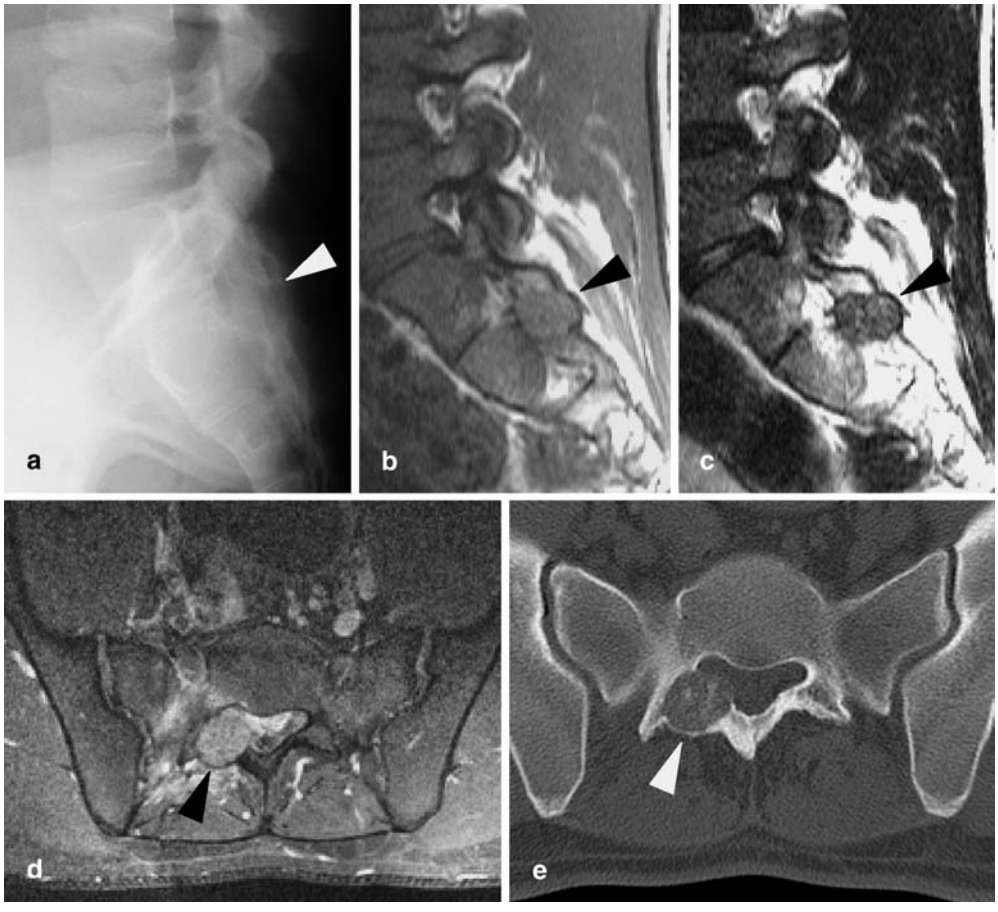

Fig. 3a–e Osteoblastoma of the sacrum in a 20-year-old man. **a** Lateral radiograph shows faint lesion of ground-glass density (*arrowhead*) at the posterior elements of the second sacral vertebra. **b** Sagittal T1-weighted SE, **c** sagittal T2-weighted FSE, and **d** axial contrast-enhanced fat-suppressed T1-weighted SE MR images reveal a well-defined tumor (*arrowheads*) originating from the arch of the second sacral vertebra. Note rim of low signal intensity at the periphery of the lesion, hypointensity of tumor tissue with T2-weighting, and marked contrast enhancement of tumor tissue as well as adjacent bone marrow and soft tissue edema. On **e** axial CT scan cortical expansion (*arrowhead*), matrix mineralizations, as well as reactive sclerosis of adjacent bone are clearly demonstrated

to the shell-like periosteal reaction seen on CT scans in expansile lesions [6, 15], MR imaging can demonstrate a rim of low signal intensity at the periphery of the nidus (Fig. 3). As in osteoid osteoma, reactive edema of adjacent bone marrow and soft tissues is usually present [12, 15, 16]. Cystic areas with contrast-enhancing walls and/or fluid levels are occasionally observed in osteoblastomas with a secondary aneurysmal bone cyst component. In the spine, MR imaging can demonstrate epidural or paraneural tumor extent but tends to overestimate the size of the lesion [16]. The amount of bone destruction and the anatomic relationship of the lesion to the posterior vertebral elements are often more clearly defined on CT, and therefore, CT is usually preferred in preoperative imaging [6, 12, 15, 16].

Enchondroma and osteochondroma

Enchondromas represent incidental findings on plain radiographs in more than 50% of the cases. These intramedullary lesions are most commonly detected in the short tubular bones of the hand and the (dia)metaphyses of the femur, humerus, and tibia [1, 17]. In asymptomatic cases with typical radiographic appearance further diagnostic workup is usually not required. Pain, which can be directly attributed to the lesion and which cannot be explained by pathologic fracture, on the other hand, should raise the suspicion for malignancy [4, 17, 18]; however, the distinction of enchondroma and (primary or secondary) central chondrosarcoma represents a major diagnostic dilemma, especially if the chondrosarcoma is a well-differentiated (low-grade) lesion [18, 19]. Plain radiographs generally do not allow an accurate differentiation of benign and low-grade malignant cartilaginous tumors, and the diagnostic value of biopsies is severely affected by sample errors due to tumor heterogeneity [17, 18, 19].

Computed tomography can aid in the diagnosis of a cartilaginous tumor by demonstrating lobulated margins and the typical patterns of mineralized chondroid matrix (Fig. 4) [4]. Most morphologic findings which have been used to diagnose a central chondrosarcoma, with the exception of epiphyseal or axial location and a lesion size >5–6 cm [18, 19], represent alterations of the cortex. Expansion of a major bone with cortical remodeling, periosteal reactions, cortical thickening, and, most importantly, deep endosteal scalloping (more than two-thirds of cortical thickness), as well as complete cortical pene-

Fig. 4a–e Enchondroma of the tibia in a 42-year-old woman. **a** Anteroposterior radiograph shows central osteolytic lesion (*arrowhead*) with endosteal cortical scalloping and chondrogenous matrix calcifications. **b** Coronal T1-weighted SE, **c** coronal STIR, and **d** axial T2-weighted FSE MR images demonstrate a lobulated lesion of low signal intensity on T1- and high signal intensity on STIR- and T2-weighted images. The extent of endosteal erosion of the cortex is overestimated on MR images compared with **e** corresponding CT scan. Matrix mineralization is also much more clearly depicted on CT image. Histologic examination of curretted material (not shown) confirmed the diagnosis of an enchondroma

tration (Fig. 5), have all been reported to represent indicators of malignancy and can clearly be demonstrated by CT [17, 18].

Magnetic resonance imaging, in our experience, is less reliable in assessment of cortical erosion and penetration, especially if the cortex involved originally is relatively thin (Fig. 5); however, MR can be very helpful in cases where the diagnosis of a chondroma is questionable. Well-differentiated cartilaginous tumors typically show a lobular configuration, low signal intensity on T1-, and high signal intensity on T2-weighted images (Fig. 4). Contrast-enhanced images can demonstrate a characteristic "ring-and-arc"-like enhancement pattern, which histologically corresponds with fibrovascular tissue at the periphery of avascular lobules of hyaline cartilage [20, 21]. The presence of hypointense septa on T2-weighted images and "septal" enhancement on gadolinium-enhanced T1-weighted images are features that have been controversially discussed as criteria for a low-grade chondrosarcoma [18, 21, 22, 23, 24, 25].

Osteochondromas (osteocartilaginous exostoses), which represent the most common (10–15%) of all bone tumors, can usually be sufficiently diagnosed on radiographs [1, 4, 24]. The majority of osteochondromas are asymptomatic and therefore are discovered incidentally during childhood. Painfulness in the absence of fracture or mechanical irritation of adjacent structures or growth of an osteochondroma in the skeletal mature patient should alert to the possibility of malignant transformation [1, 4, 24, 26]. Malignant transformation is derived from the cartilaginous component of the lesion (cartilage cap) and is thought to occur in approximately 1% of patients with a solitary osteochondroma and 5–25% of patients with multiple lesions (hereditary multiple exostoses) [1, 4, 24, 26]. The resulting malignant tumor most commonly is a low-grade chondrosarcoma [24, 26].

Malignant transformation of an osteochondroma is very likely, if the thickness of the cartilage cap exceeds 2 cm in adults and 3 cm in children [1, 24, 27]. Magnetic resonance imaging (Figs. 6, 7) represents the most reliable method in measuring cartilage cap thickness [24, 27, 28], whereas CT shows a tendency for underestimation [29], and ultrasound can be limited by the anatomic localization and orientation of the osteochondroma [24, 28].

Fast dynamic gradient-echo (GRE) MR imaging has been reported to allow differentiation of enchondromas and osteochondromas from chondrosarcomas on the basis of onset and patterns of gadolinium enhancement [21]; however, since the study performed by Geirnaerdt and coworkers [21] showed an overlap in early enhancement patterns of chondrosarcomas and osteochondromas in the immature skeleton, and less than 50% of the included chondrosarcomas were grade-1 lesions [21], the usefulness of this technique in distinction of benign and low-grade malignant cartilaginous tumors should be further evaluated in a large patient population [18, 24].

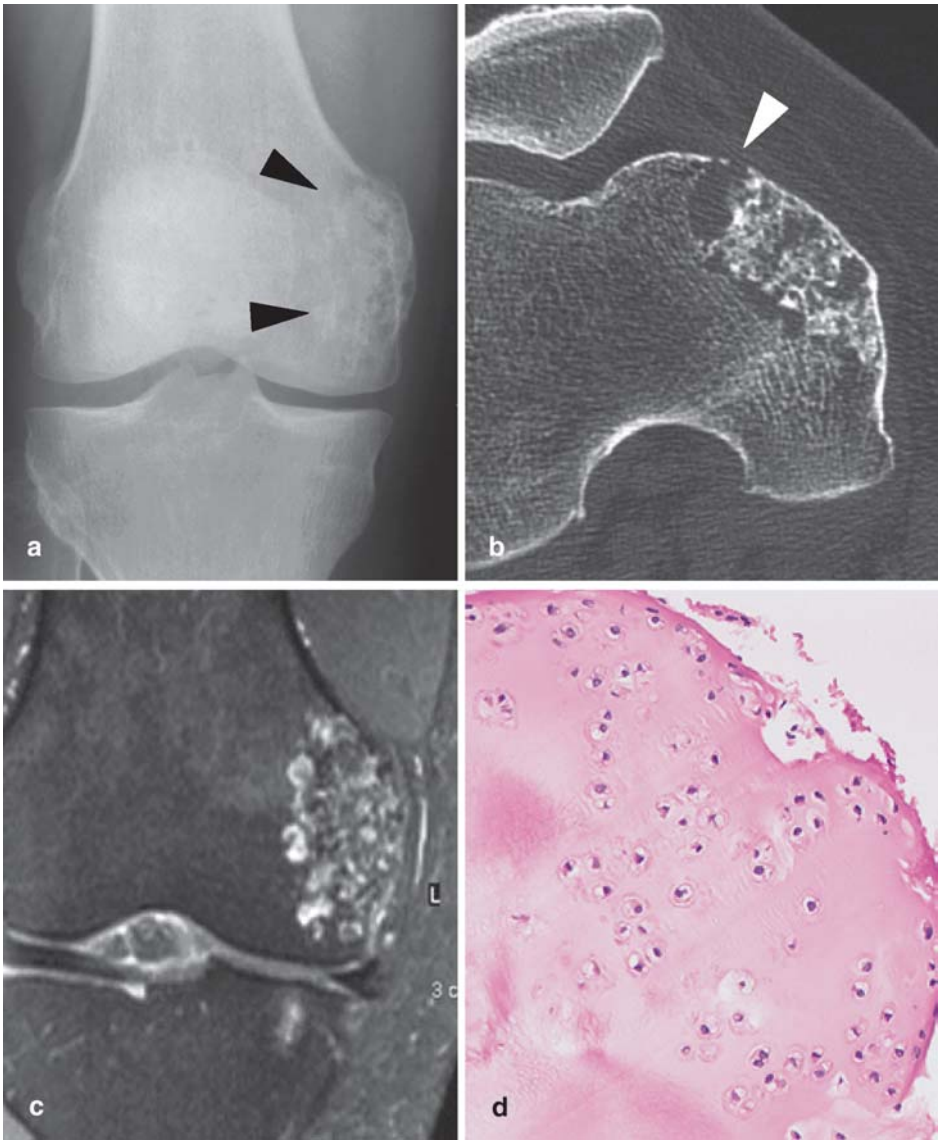

Fig. 5a–d Low-grade central chondrosarcoma of the femur in a 44-year-old woman. **a** Anteroposterior radiograph shows an osteolytic lesion (*arrowheads*) with matrix calcifications in the lateral femoral condyle. **b** The CT scan depicts relatively irregular margins, chondrogenous matrix calcifications, as well as focal penetration of the cortex (*arrowhead*), which, in addition to epiphyseal location, strongly suggests a chondrosarcoma. On **c** coronal fat-suppressed T2-weighted FSE MR image the lesions shows a lobular appearance and high signal intensity of non-mineralized matrix. Cortical alterations are not clearly demonstrated. **d** Histologic section (hematoxylin and eosin stain) from biopsy specimen shows a lobule of hyaline cartilage with atypic chondrocytes, consistent with the diagnosis of a grade-1 chondrosarcoma

Intraosseous lipoma

Intraosseous lipomas are thought to represent very rare lesions accounting for only 0.1–2.5% of all bone tumors; however, since these lesions are most often asymptomatic, their true incidence is probably higher [1]. Especially when located in the calcaneus or the proximal femur, intraosseous lipomas often present with pathognomonic radiographic features [4]; otherwise, they can mimic fibro-osseous lesions, simple or aneurysmal bone cysts, as well as cartilaginous tumors [30]. On rare occasions lipomas can originate from the periosteum or the parosteal soft tissues and can cause cortical erosion, hyperostosis, or periostitis, which might result in a misleading radiographic appearance simulating osteochondroma or other surface lesions [1, 4, 30].

Computed tomography and MR imaging (Fig. 8) can both be used to verify the fatty component of the tumors, although the cross-sectional imaging appearance of intraosseous lipomas varies with their histologic stage [30]. Solid lesions consisting of viable lipocytes (stage 1) present with similar attenuation values and signal intensities compared with subcutaneous fat. Stage-2 lipomas show partial fat necrosis and focal calcifications as well as areas of viable fat (Fig. 8). In stage-3 lipomas extensive liponecrosis with variable degrees of cyst formation, calcification, and new bone formation is seen. At this stage residual fatty tissue might only be detected at the periphery of the lesions [1, 30].

In general, cross-sectional imaging should only be performed to confirm the diagnosis in doubtful cases in order to obviate the need for biopsy.

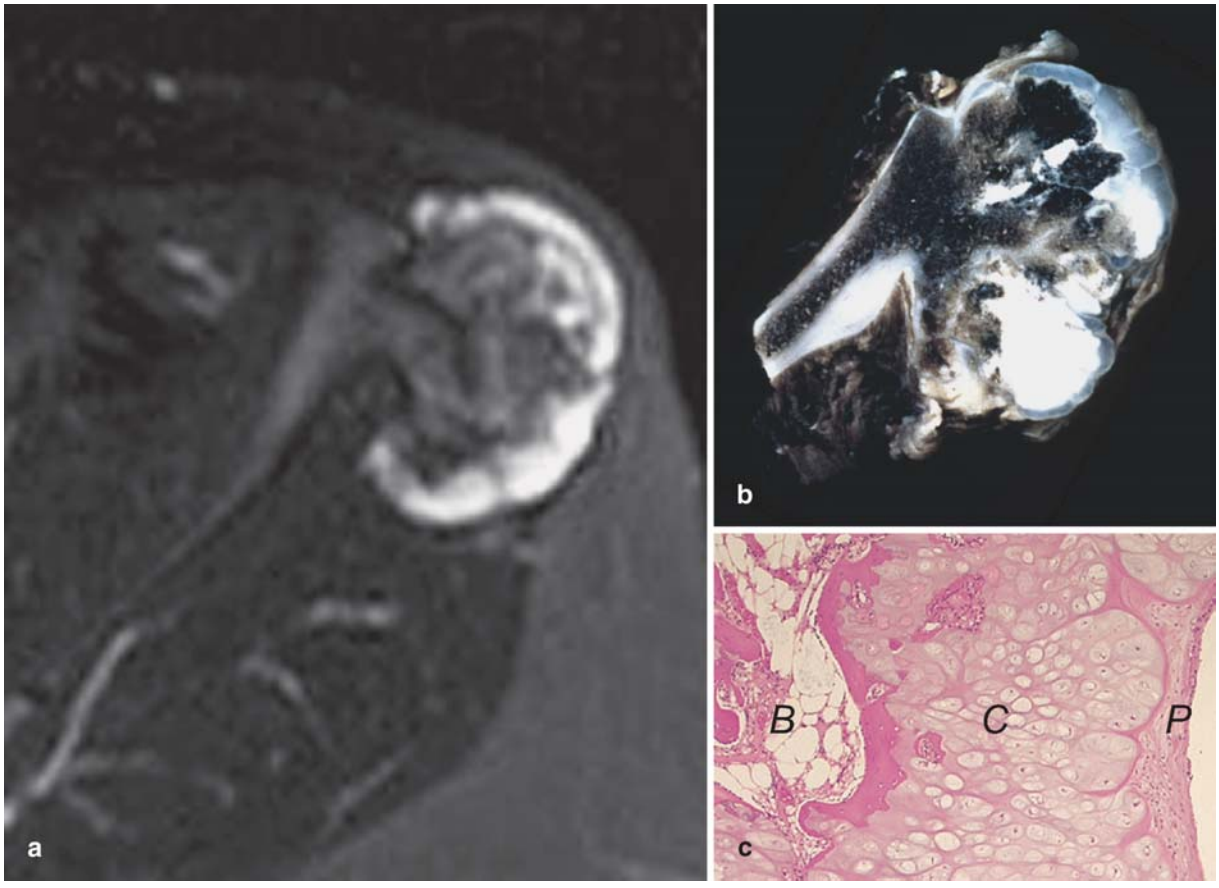

Fig. 6a–c Solitary osteochondroma of the ilium in a 22-year-old woman. **a** Axial fat-suppressed T2-weighted FSE MR image shows continuity of the exostotic cortex and bone marrow with that of the iliac wing. The cartilage cap typically demonstrates high signal intensity and a hypointense superficial lining with T2-weighted pulse sequences. **b** Corresponding macrosection of resected specimen shows classic morphology of an osteochondroma. **c** Histologic section (hematoxylin and eosin stain) shows hyaline cartilage of the cap (*C*) morphologically resembling that of a physeal growth plate, covered by perichondrium (*P*). *B* cancellous bone of the stalk

Hemangioma

More than 75% of hemangiomas of bone are located in the spine and the skull, approximately 10% in long bones, and approximately 5% in the ribs, with the cavernous and capillary form being the most frequent histologic subtypes [1]. The majority of vertebral hemangiomas are detected incidentally on radiography or MR imaging. Whereas hemangiomas of the spine and skull usually have an almost pathognomonic radiographic appearance, those located in long or flat bones may cause problems in differential diagnosis [4]. In long tubular bones, the lesion most often occur intramedullary but may also originate from the cortex or periosteum, and like in the spine, they even may demonstrate simultaneous involvement of bone and adjacent soft tissues [1, 4].

The variable proportions of vascular and lipomatous soft tissue elements influence the MR appearance of hemangiomas. Lesions with a predominantly fatty matrix show high signal intensity on T1-, intermediate to high signal intensity on T2-, and a loss of signal on STIR- or fat-suppressed T2-weighted images. If the vascular elements predominate, the lesions appear hypointense on T1- and extremely hyperintense on STIR- and T2-weighted images. Accordingly, contrast-enhancement within the lesions may be moderate to marked [4, 31]. MR imaging can be helpful in establishing the diagnosis in doubtful cases, in definition of intraosseous extent, and in detection of simultaneous soft tissue involvement (Fig. 9). Since predominantly vascular hemangiomas of the spine are more likely to undergo progredient expansion, development of a soft tissue mass, and to cause vertebral instability, MR characteristics are thought to represent useful indicators of aggressive behavior [31].

In lesions with inconclusive radiographic findings, CT may at times allow the recognition of typical patterns of hemangiomatous bone destruction, such as the “honeycomb,” “soap bubble,” or “sunburst” appearance [1, 4]. CT can also be used in differentiation of predominantly lipomatous or vascular lesions [31]; however, it

Fig. 7a–d Exostotic chondrosarcoma of the femur in a 31-year-old man. **a** Anteroposterior radiograph shows an osseous outgrowth (*arrowhead*) originating from the distal femoral metaphysis as well as irregular calcifications (*arrow*). **b** Coronal T1-weighted SE, **c** axial fat-suppressed T2-weighted FSE, and **d** contrast-enhanced fat-suppressed T1-weighted SE MR images show an osseous stalk (*arrowheads*) and an overlying cartilage cap (*arrows*) with a maximum thickness of 3.5 cm. The cap demonstrates typical MR characteristics of hyaline cartilage with hypointense signal on T1- and hyperintense signal on T2-weighted images. Note hypointense septa as well as "ring-and-arc" and "septal" pattern of contrast enhancement. Histology confirmed a grade-1 chondrosarcoma arising in an osteochondroma

represents the most valuable method in demonstrating the severity of bone loss of the vertebral elements in symptomatic vertebral hemangiomas [4], and therefore can effectively aid in planning and guidance of therapeutic interventions.

Giant cell tumor

Giant cell tumor (GCT) represents a relatively common osseous neoplasm accounting for up to 10% of all bone tumors. Due to its aggressive growth it has been termed semimalignant; however, in the majority of cases (>90%) GCT is histologically benign and occurs as a solitary, typically epimetaphyseal lesion [1, 4, 32].

Although CT can help to demonstrate cortical expansion or penetration, trabeculations, absence of matrix mineralization, and pathologic fracture [32], radiographs are usually sufficient to establish the diagnosis, particularly if the tumor is located in a long tubular bone. GCTs of the spine and pelvis are relatively rare [1, 4, 12, 32].

As with other bone tumors, MR imaging is superior to CT in delineation of soft tissue extension, which can be observed in GCT in more than one-third of cases, as well as joint involvement (Fig. 10) [32].

On MR images, GCT usually presents as a well-defined lesion, which can be marginated by a rim of low signal intensity (Fig. 10) representing either reactive osteosclerosis or a fibrous pseudocapsule [32]. Although signal characteristics of solid tissue in GCT can be unspecific, many lesions (63–96%) predominantly reveal moderate to marked hypointensity on T1- as well as T2-weighted images, a feature that has been attributed to the presence of hemosiderin deposits and/or high collagen content, and that can be useful in excluding other lesions occurring in an epiphyseal location, such as intraosseous

Fig. 8a–d Intraosseous lipoma of the femur in a 33 year-old man. **a** Anteroposterior radiograph shows a well-defined eccentric osteolytic lesion of the distal femoral metaphysis with ballooning of the medial cortex, trabeculations, and a focal calcification (*arrowhead*). On **b** sagittal T1-weighted SE, **c** coronal T2-weighted FSE, and **d** axial fat-suppressed T2-weighted FSE MR images the lesion demonstrates signal intensities similar to that of subcutaneous fat. Small cystic areas (*arrows*) as well as calcifications (*arrowheads*) are consistent with the diagnosis of a stage-2 lipoma

ganglion, subchondral cyst, chondroblastoma, and clear cell chondrosarcoma [12, 32, 33]. GCTs often demonstrate cystic components on MR images, which can develop due to hemorrhage or formation of a secondary aneurysmal bone cyst (Fig. 10) [32]. Biopsy should be directed to the solid tissue component, where diagnostic tissue is much more likely to be obtained [1, 32, 34].

Aneurysmal bone cyst

Aneurysmal bone cyst (ABC) can occur as a primary lesion or secondary to other bone lesions, such as GCT, osteoblastoma, or chondroblastoma. The primary form accounts for approximately two-thirds of the cases. It is almost exclusively found in children and young adults and shows a predilection for the long tubular bones and the spine [2, 4, 12, 34, 35, 36]. The classic radiographic appearance of ABC has been extensively described in the literature [4, 12, 36]; however, in approximately 40% of the cases radiographs have been reported to be either inconclusive (e.g., due to location at sites of complex skeletal anatomy) or unspecific, or to reveal aggressive features suggesting malignancy [35, 37].

In addition to radiography, MR imaging represents the most informative diagnostic modality, since it has the potential to demonstrate the pathologic anatomy of ABC, independent from its location within the skeleton or within a specific bone [12, 34, 36, 37]. The typical MR appearance of ABC (Fig. 11) is that of an expansile lesion consisting of multiple cystic spaces frequently lined by a rim of low signal intensity, which represents fibrous tissue. In the majority of cases multiple fluid levels caused by sedimentation of non-coagulated blood com-

Fig. 9a, b Hemangioma of the tibia in a 22-year-old woman. **a** Lateral radiograph shows a longitudinally oriented lytic lesion with a trabecular pattern (*arrowheads*) in the shaft of the tibia. **b** Axial T2-weighted SE MR image demonstrates tubular structures of high signal intensity (*arrowheads*) in the tibia as well as in the adjacent soft tissues, representing intra- and extraosseous vascular components of a hemangioma with slow blood flow. Note hypertrophy of the draining anterior tibial veins (*arrow*)

Fig. 10a–d Giant cell tumor of the femur in 29-year-old man. **a** Anteroposterior radiograph shows an epimetaphyseal osteolytic lesion which completely penetrates the cortex at the medial aspect of the femoral head and neck. **b** Coronal T1-weighted SE, **c** corresponding contrast-enhanced T1-weighted SE, and **d** axial T2-weighted SE MR images show an inhomogeneous tumor which invades the joint (*arrowheads*). The lesion is marginated by a rim of low signal intensity and demonstrates inhomogeneous contrast enhancement. Cystic areas with fluid levels seen on T2-weighted image (**d**) histologically corresponded with a secondary aneurysmal bone cyst component

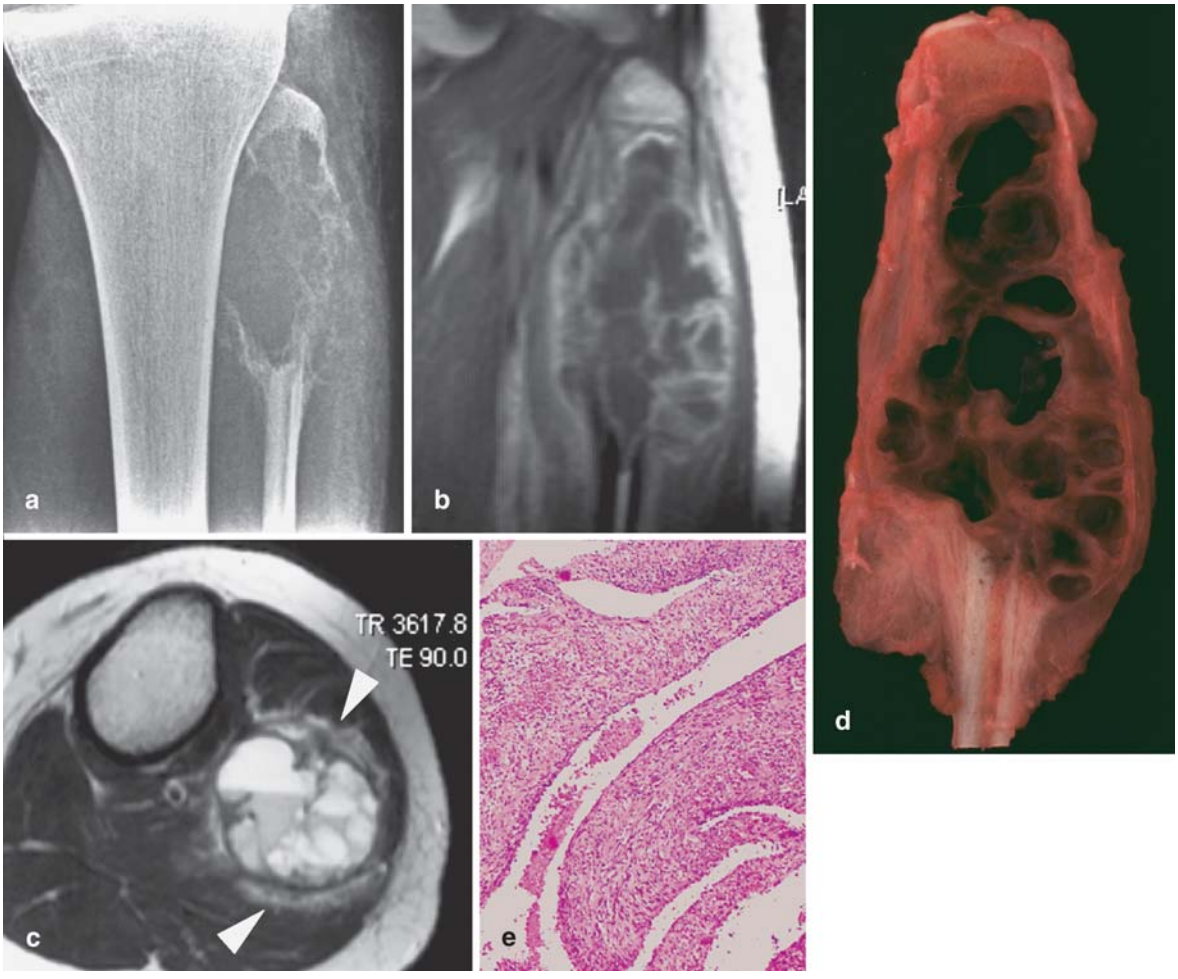

Fig. 11a–e Aneursymal bone cyst of the fibula in a 16-year-old female. **a** Anteroposterior radiograph shows a highly aggressive lytic lesion of the proximal fibular meta/diaphysis with a bizarre interrupted periosteal reaction. **b**, **c** MR demonstrates an expansile, exclusively cystic lesion with contrast-enhancing walls and internal septations on **b** coronal contrast-enhanced T1-weighted SE image, and a rim of low signal intensity as well as multiple fluid levels on **c** axial T2-weighted FSE image. Note edema of adjacent soft tissues (*arrowheads*). **d** Corresponding macrosection of resected specimen shows a sponge-like lesion consisting of multiple, variably sized cystic cavities. **e** Histologic section (hematoxylin and eosin stain) demonstrates red blood cells surrounded by typical cyst walls with a pseudoendothelial lining and a fibrous stroma containing giant cells and dilated capillaries

ponents can be detetcted especially on T2-weighted images [34, 37]. Fluid levels in general are not specific for ABC but make the diagnosis very likely, particularly if the entire lesion is composed of cystic cavities [12, 34, 36, 38]. Contrast-enhanced T1-weighted sequences show enhancement of cyst walls and internal septations which on histologic examinations typically contain dilated capillaries [34]. In almost one-third of cases MR images reveal edema of soft tissues especially adjacent to lesions with marked expansivity or location at or close to the bone surface [34, 37]. Besides cystic spaces, primary ABC can contain relevant portions of solid material, which can usually be identified by MR imaging [34]; however, the presence of a solid tissue component should alert to the most important differential diagnoses, teleangiectatic osteosarcoma, and secondary ABC [34, 38]. In this case, MR should be used to guide biopsy in order to harvest material from the solid portion of the lesion [34].

In our experience and that of other authors [12], CT is less sensitive in demonstrating the internal features of ABC. In the series by Hudson, fluid levels were detected at CT in only 35% of the lesions [39]. As an additional modality, CT may be beneficial for demonstration of complex anatomic relationships in lesions located in the spine or pelvis.

Simple bone cyst

Especially in long tubular bones the radiographic appearance of a simple bone cyst is characteristic in the vast majority of cases, and further imaging studies are unnec-

Fig. 12a–e Eosinophilic granuloma (Langerhans' cell histiocytosis) of the tibia in a 7-year-old boy. **a** Anteroposterior radiograph shows an intramedullary osteolytic lesion of the tibial diaphysis accompanied by a subtle lamellar periosteal reaction (*arrowhead*). **b**, **c** MR imaging reveals an oval lesion (*arrowheads*) within the bone marrow of the tibia with hypointense signal on **b** sagittal T1-weighted SE image and hyperintense signal on **c** sagittal STIR image, surrounded by a zone of extensive edema. **d** Axial fat-suppressed T2-weighted FSE MR image reveals circular periosteal and parosteal edema, but absence of a soft tissue mass. **e** Photomicrograph of histologic section (hematoxylin and eosin stain) shows histocyte-like cells (Langerhans' cells) and dense infiltrates of eosinophils

essary [2, 4]. Computed tomography at times may be helpful in identification of pathologic fracture or a "fallen fragment," and can be used in evaluation of the extent of the lesion in anatomically complex areas such as the pelvis [4]. Both, CT and MR imaging, can verify the cystic character of the lesion. Compared with aneurysmal bone cysts, fluid levels and internal septations represent significantly less frequent MR findings in simple (unicameral) bone cysts [34, 40].

Eosinophilic granuloma

Eosinophilic granuloma (Langerhans' cell histiocytosis) as a solitary bone lesion represents the most common manifestation of Langerhans' cell histiocytosis, typically occurring in children between 5 and 10 years of age. Additional bone lesions are detected in only 10–20% of the patients who initially present with a solitary granuloma. The skull, femur, vertebrae, pelvis, and ribs are the most common sites of involvement. Radiographic findings in eosinophilic granuloma are usually unspecific with the most important differential diagnosis being Ewing's sarcoma, osteomyelitis, and osteblastoma [2].

On MR examinations eosinophilic granuloma presents as an intramedullary tumor with hypointense T1- and hyperintense T2-weighted signal intensity, which corresponds with the lytic lesion seen on radiographs (Fig. 12). Especially early-stage lesions are often accompanied by edema of adjacent bone marrow, periosteum, and soft tis-

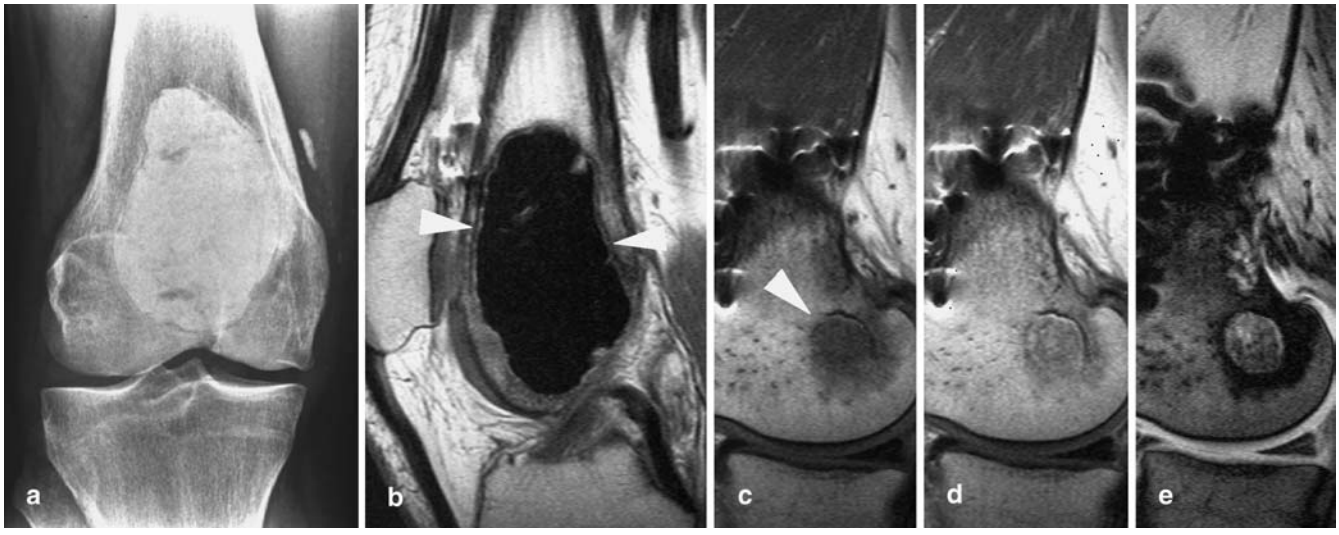

Fig. 13a–e Postoperative recurrence of giant cell tumor following curettage and bone cement (PMMA) filling in a 28-year-old man. **a** Anteroposterior radiograph shows epimetaphyseal defect filled with bone cement. Note normal radiolucent zone at the bone–cement interface. **b** Midsagittal contrast-enhanced T1-weighted SE image demonstrates delicate rim of contrast-enhancing granulation tissue at the bone–cement interface (*arrowheads*), which represents a normal finding following PMMA filling. **c** More medial sagittal T1-weighted SE image depicts a nodular mass partially marginated by a rim of low signal intensity (*arrowhead*). The tumor tissue demonstrates inhomogeneous enhancement on **d** corresponding contrast-enhanced image, as well as areas of low signal intensity on **e** T2*-weighted GRE image. Histology (not shown) confirmed recurrence of giant cell tumor at the bone–cement interface

sues [41, 42, 43]. T1-weighted pulse sequences following gadolinium administration usually show diffuse enhancement of the lesion as well as the surrounding reactive changes [43]. An endosteal rim of low signal intensity at the periphery of the main lesion, which might be observed on STIR images, has been reported to represent a possible indicator of initial healing [41]. The MR appearance of eosinophilic granuloma is unspecific and does not allow a clear distinction from osteoblastoma and osteomyelitis. Ewing's sarcoma, as the most worrisome differential diagnosis, usually demonstrates more extensive peritumoral edema [41] as well as a larger extraosseous soft tissue component. In our experience, the diagnosis of eosinophilic granuloma can often be established by the combination of patient age, laboratory, radiographic, and MR imaging findings.

Tumor-related complications

Except pathologic fracture, complications associated with benign bone lesions are most commonly caused by mass effects. Compression of the spinal cord or nerve roots with consecutive neurologic symptoms is frequently seen with spinal ABC, osteoblastoma, and osteochondroma [12, 24] and can most clearly be demonstrated by MR imaging [3, 4, 24]. Neurologic symptoms due to deformation of the skull are typical sequelae of craniofacial fibrous dysplasia. Computed tomography is the most valuable method in defining the degree of craniofacial bone involvement related to the patients' symptoms [4]. Various complications caused by compression, mechanical irritation, or injury of adjacent soft tissues, arterial and venous vessels, and peripheral nerves have been described with osteochondromas [4, 24]. Magnetic resonance imaging has been reported to be the most informative method in evaluation of symptomatic osteochondromas, since it allows distinction of different compression syndromes, bursa formation, and malignant transformation [24].

Postoperative recurrence

Imaging of postoperative recurrence of benign bone lesions basically follows the same principles as imaging of the primary lesions. Special considerations have to be made in the diagnosis of recurrent GCT, ABC, osteoid osteoma, and benign cartilage-forming tumors.

Postoperative recurrence represents a major problem in patients with GCTs and ABCs. Both lesions show a high recurrence rate within the first 2–3 years after initial treatment [32, 33, 34, 35, 44]. Early detection of postoperative recurrence of these relatively rapid growing lesions is of great importance in order to avoid further loss of bone substance and to allow once again surgical intervention with preservation of stability and function of the affected skeletal elements [44]. Radiographs are of limited value in early detection of tumor recurrence, since new areas of bone destruction can be obscured by sequelae of previous surgery, bone cement, bone grafts, or simply due

to the limitations of two-dimensional imaging. Both, CT and MR imaging, are helpful in identification of small areas of progressive bone destruction [32, 44] and therefore should additionally be performed in the first 2 years of follow-up, even if radiographs are unremarkable.

Computed tomography has the ability to depict initial new bone destruction at the interface between bone cement and bone after polymethylmethacrylate (PMMA) filling, which has to be distinguished from the normal radiolucent zone of 1–2 mm thickness that often develops due to PMMA retraction and the cytotoxic effect of its exothermic reaction, and which usually does not progress after 6 months postoperatively [32, 44]. Furthermore, CT can show tumor-related resorption of bone grafts much earlier than radiographs; however, in our experience, MR imaging is more specific in differentiation of early recurrence of GCT or ABC from postoperative sequelae, such as formation of granulation tissue at a bone–cement interface or heterogeneous marrow changes seen in incomplete bone graft incorporation [32], because the signal characteristics and/or morphologic features of the recurrent lesions are often similar to those of the original lesions (Fig. 13).

Recurrence of an osteoid osteoma after surgical resection or percutaneous treatment is characterized by persistence or recurrence of pain [10, 45]. Like the primary lesion, recurrent osteoid osteoma can most reliably be verified by CT, which shows a persistent, incompletely ossified, or, rarely, a new nidus [10, 45]. Dynamic CT or MR imaging can help to identify the site of the recurrence, when inhomogeneous areas of ostesclerosis and radiolucency hinder exact localization on static images [45].

Enchondromas and osteochondromas rarely recur after surgical treatment by thorough currettage and complete resection, respectively (2–10%) [1]. Recurrent tumors usually arise from hyaline cartilage or perichondrium (osteochondroma) left behind [1, 24, 27]. Especially in osteochondromas, where recurrence occurs within the soft tissues, MR imaging represents the most valuable imaging modality, because it has the potential to demonstrate typical morphologic features of a cartilage-forming lesion in the recurrent tumor [24].

References

1. Forest M, Coindre JM, Diebold J (1997) Pathology of tumors. In: Forest M, Tomeno B, Vanel D (eds) Orthopedic surgical pathology: diagnosis of tumors and pseudotumoral lesions of bone and joints. Churchill Livingstone, Edinburgh, pp 71–516
2. Forest M, Amouroux J (1997) Pathology of pseudotumoral lesions. In: Forest M, Tomeno B, Vanel D (eds) Orthopedic surgical pathology: diagnosis of tumors and pseudotumoral lesions of bone and joints. Churchill Livingstone, Edinburgh, pp 519–670
3. Resnick D (1995) Tumors and tumor-like lesions of bone: radiographic principles. In: Resnick D (ed) Diagnosis of bone and joint disorders. Saunders, Philadelphia, pp 3613–3627
4. Resnick D, Kyriakos M, Greenway GD (1995) Tumors and tumor-like lesions of bone: imaging and pathology of specific lesions. In: Resnick D (ed) Diagnosis of bone and joint disorders. Saunders, Philadelphia, pp 3628–3938
5. Magid D (1993) Two-dimensional and three-dimensional computed tomographic imaging in musculoskeletal tumors. Radiol Clin North Am 31:425–447
6. Bloem JL, Kroon HM (1993) Imaging of bone and soft tissue tumors: osseous lesions. Radiol Clin North Am 31:261–278
7. Berquist TH (1993) Magnetic resonance imaging of primary skeletal neoplasms. Radiol Clin North Am 31:411–424
8. Kransdorf MJ, Stull MA, Gilkey FW, Moser RP (1991) Osteoid osteoma. Radiographics 11:671–669
9. Assoun J, Richardi G, Railhac JJ et al. (1994) Osteoid osteoma: MR imaging versus CT. Radiology 191:217–223
10. Woertler K, Vestring T, Boettner F, Winkelmann W, Heindel W, Lindner N (2001) Osteoid osteoma: CT-guided percutaneous radiofrequency ablation and follow-up in 47 patients. J Vasc Interv Radiol 12:717–722
11. Davies M, Cassar-Pullicino VN, Davies AM, McCall IW, Tyrrell PNM (2002) The diagnostic accuracy of MR imaging in osteoid osteoma. Skeletal Radiol 31:559–569
12. Murphey MD, Andrews CL, Flemming DJ, Temple HT, Smith WS, Smirniotopoulos JG (1996) Primary tumors of the spine: radiologic–pathologic correlation. Radiographics 16:1131–1158
13. McGrath BE, Bush CH, Nelson TE, Scarborough MT (1996) Evaluation of suspected osteoid osteoma. Clin Orthop 327:247–252
14. Levine E, Neff JR (1983) Dynamic computed tomography scanning of benign bone lesions: preliminary results. Skeletal Radiol 9:238–245
15. Kroon HM, Schurmans J (1990) Osteoblastoma: clinical and radiologic findings in 98 new cases. Radiology 175:783–790
16. Shaikh MI, Saifuddin A, Pringle J, Natali C, Sherazi Z (1999) Spinal osteoblastoma: CT and MR imaging with pathological correlation. Skeletal Radiol 28:33–40
17. Brien EW, Mirra JM, Kerr R (1997) Benign and malignant cartilage tumors of bone and joint: their anatomic and theoretical basis with an emphasis on radiology, pathology and clinical biology. I. The intramedullary cartilage tumors. Skeletal Radiol 26:325–353
18. Murphey MD, Flemming DJ, Boyea SR, Bojescul JA, Sweet DE, Temple HT (1998) Enchondroma versus chondrosarcoma in the appendicular skeleton: differentiating features. Radiographics 18:1213–1237
19. Geirnaerdt MJA, Hermans J, Bloem JL, Kroon HM, Pope TL, Taminiau AHM, Hogendoorn PC (1997) Usefulness of radiography in differentiating enchondroma from central grade 1 chondrosarcoma. Am J Roentgenol 169:1097–2004
20. Aoki J, Sone S, Fujioka F et al. (1991) MR of enchondroma and chondrosarcoma: rings and arcs of Gd-DTPA enhancement. J Comput Assist Tomogr 15:1011–1016
21. Geirnaerdt MJA, Hogendoorn PCW, Bloem JL, Taminiau AHM, van der Woude HJ (2000) Cartilaginous tumors: fast contrast-enhanced MR imaging. Radiology 214:539–546

22. De Beuckeleer LHL, De Schepper AMA, Ramon F (1996) Magnetic resonance imaging of cartilaginous tumors: Is it useful or necessary? Skeletal Radiol 25:137–141
23. De Beuckeleer LHL, De Schepper AMA, Ramon F, Somville J (1995) Magnetic resonance imaging of cartilaginous tumors: a retrospective study of 79 patients. Eur J Radiol 21:34–40
24. Woertler K, Lindner N, Gosheger G, Brinkschmidt C, Heindel W (2000) Osteochondroma: MR imaging of tumor-related complications. Eur Radiol 10:823–840
25. Geirnaerdt MJA, Bloem JL, Eulderink F, Hogendoorn PCW, Taminiau AHM (1993) Cartilaginous tumours: correlation of gadolinium-enhanced MR imaging and histopathologic findings. Radiology 186:813–817
26. Brien EW, Mirra JM, Luck JV (1999) Benign and malignant cartilage tumors of bone and joint: their anatomic and theoretical basis with an emphasis on radiology, pathology and clinical biology. II. Juxtacortical cartilage tumors. Skeletal Radiol 28:1–20
27. Lee JK, Yao L, Wirth CR (1987) MR imaging of solitary osteochondroma: report of eight cases. Am J Roentgenol 149:557–560
28. Malghem J, Vande Berg B, Noel H, Maldague B (1992) Benign osteochondromas and exostotic chondrosarcoma: evaluation of cartilage cap thickness by ultrasound. Skeletal Radiol 21:33–37
29. Hudson TM, Springfield DS, Spanier SS, Enneking WF, Hamlin DJ (1984) Benign exostoses and exostotic chondrosarcomas: evaluation of cartilage thickness by CT. Radiology 152:595–599
30. Propeck T, Bullard MA, Lin J, Doi K, Martel W (2000) Radiologic–pathologic correlation of intraosseous lipomas. AJR 175:673–678
31. Laredo JD, Assouline E, Gelbert F, Wybier M, Merland JJ, Tubiana JM (1990) Vertebral hemangiomas: fat content as a sign of aggressiveness. Radiology 177:467–472
32. Murphey MD, Nomikos GC, Flemming DJ, Gannon FH, Temple HT, Kransdorf MJ (2001) Imaging of giant cell tumor and giant cell reparative granuloma of bone: radiologic–pathologic correlation. Radiographics 21:1283–1309
33. Aoki J, Tanikawa H, Ishii K, Seo GS, Karakida O, Sone S, Ichikawa T, Kachi K (1996) MR findings indicative of hemosiderin in giant-cell tumor of bone: frequency, cause, and diagnostic significance. Am J Roentgenol 166:145–148
34. Woertler K, Blasius S, Hillmann A, Brinkschmidt C, Heindel W (2000) MR morphology of primary aneurysmal bone cyst: a retrospective analysis of 38 cases. Rofo Fortschr Rontgenstr 172:591–596
35. Vergel de Dios AM, Bond JR, Shives TC, McLeod RA, Unni KK (1992) Aneurysmal bone cyst: a clinicopathologic study of 238 cases. Cancer 69:2921–2931
36. Kransdorf MJ, Sweet DE (1995) Aneurysmal bone cyst: concept, controversy, clinical presentation, and imaging. Am J Roentgenol 164:573–580
37. Woertler K, Brinkschmidt C (2002) Imaging features of subperiosteal aneurysmal bone cyst. Acta Radiol 43:336–339
38. Murphey MD, Flemming DJ, Torop AH, Smith SE, Sonin AH, Temple HT (1998) Imaging differentiation of primary and secondary aneurysmal bone cyst with pathologic correlation. Radiology 209:311
39. Hudson TM (1984) Fluid levels in aneurysmal bone cyst: a CT feature. Am J Roentgenol 142:1001–1004
40. Sullivan RJ, Meyer JS, Dormans JP, Davidson RS (1999) Diagnosing aneurysmal and unicameral bone cysts with magnetic resonance imaging. Clin Orthop 366:186–190
41. Davies AM, Pikoulas C, Griffith J (1994) MRI of eosinophilic granuloma. Eur J Radiol 18:205–209
42. Beltran J, Aparisi F, Bonmati LM, Rosenberg ZS, Present D, Steiner GC (1993) Eosinophilic granuloma: MRI manifestations. Skeletal Radiol 22:157–161
43. Monroc M, Ducou le Pointe H, Haddad S, Josset P, Montagne JP (1994) Soft tissue signal abnormality associated with eosinophilic granuloma. Correlation of MR imaging with pathologic findings. Pediatr Radiol 24:328–332
44. Remedios D, Saifuddin A, Pringle J (1997) Radiological and clinical recurrence of giant cell tumor of bone after the use of cement. J Bone Joint Surg Br 79:26–30
45. Pinto CH, Taminiau AHM, Vanderschueren GM, Hogendoorn PCW, Bloem JL, Obermann WR (2002) Technical considerations in CT-guided radiofrequency ablation of osteoid osteoma: tricks of the trade. Am J Roentgenol 179:1633–1642